IEEE Access
Multidisciplinary | Rapid Review | Open Access Journal

Received July 25, 2019, accepted August 13, 2019, date of publication August 19, 2019, date of current version September 3, 2019.

Digital Object Identifier 10.1109/ACCESS.2019.2936014

A Multi-Interval Homotopy Analysis Method Using Multi-Objective Optimization for Analytically Analyzing Chaotic Dynamics in Memristive Circuit

WEI HU[1], HAIBO LUO[2], CHUANDONG CHEN[1], AND RONGSHAN WEI[1], (Member, IEEE)
[1]College of Physics and Information Engineering, Fuzhou University, Fuzhou 350108, China
[2]Electronic Information and Control of Fujian University Engineering Research Center, Minjiang University, Fuzhou 350121, China

Corresponding authors: Wei Hu (whu@fzu.edu.cn) and Rongshan Wei (wrs08@fzu.edu.cn)

This work was supported in part by the National Natural Science Foundation of China under Grant 61404030, in part by the Natural Science Foundation of Fujian Province, China, under Grant 2018J01803, in part by the Education Research Project for Young Teachers of Education Department of Fujian Province under Grant JT180057, and in part by the Electronic Information and Control of Fujian University Engineering Research Center, Minjiang University under Grant MJXY-KF-EIC1805.

ABSTRACT Memristive nonlinear system has drawn much attention in recent years, due to its rich and complex dynamical characteristics. However, there are few studies focus on the analytical analysis of this significant system. In this paper, a novel analytical method for analyzing the chaotic trajectories of memristive circuit is proposed. This method combines *Homotopy Analysis Method* (HAM) and *Multi-objective Optimization* (MO), i.e., the convergence control parameter of traditional HAM is divided into lots of subintervals in the time domain and respectively optimized by MO, for accurately solving the Ordinary Differential Equations describing memristive circuits. Hence, this method is named by *MO-based multi-interval HAM* (MO-MIHAM). By using MO-MIHAM, we accurately tracked the chaotic trajectories of the classical Memristor-Capacitor-Inductor (MCL) circuit and current memristive Band Pass Filter (BPF) chaotic circuit. Furthermore, based on the comparisons of errors between analytical approximate solutions derived from MO-MIHAM and solutions solved by traditional homotopy-based analytical methods and by *Runge-Kutta-Fehlberg Method* (RKF45) based numerical analysis, we found that, MO-MIHAM is characterized by higher approximation accuracy and computational performance (comprehensively considering the accuracy, computational complexity and execution time by a proposed Quality Factor) among the homotopy-based analytical methods, due to the optimized convergence control parameters in subintervals. Besides this major advantage, MO-MIHAM enables both qualitative and quantitative analyses and high freedom to choose homotopy-related terms for simplicity, and it is insensitive to convergence issues. Therefore, it is a powerful tool for exploratory studies for analytically analyzing chaotic dynamics in memristive circuit.

INDEX TERMS Analytical method, chaotic dynamics, multi-interval homotopy analysis method, multi-objective optimization, memristive circuit.

I. INTRODUCTION

Chaos is a special dynamic phenomenon that widely exists in nonlinear systems. It can be described by a set of *Ordinary Differential Equations* (ODEs) [1]. In practice, chaos can be generally realized by electronic circuits including nonlinear device [2], [3]. Recently, memristor, which is a novel nanometer-scale device showing nonlinear evolution of resistance with the excitation signal, has gradually garnered extensive interests of academic and industrial communities, due to its unique nonlinear characteristics [4], [5]. The memristor-based (memristive) chaotic system has rich and complex dynamical characteristics [6]–[9], such as coexisting multiple attractors, period doubling bifurcation, and coexisting bifurcation modes, and has great potential for multiple applications in neural networks [10], [11], secure communication [9], [12], cryptography [13], [14], biology [15], [16], etc.

The associate editor coordinating the review of this article and approving it for publication was Woorham Bae.

Along with studies in the applications of memristive chaotic circuits, novel mathematical methods for accurately tracking the chaotic trajectories are urgently needed. Based on the authors' observations, many studies have been performed by using numerical methods so far [12]–[14], [17]–[20], restricting the studies to quantitative analyses of chaos. Even worse, it is well known that numerical methods are sensitive to convergence issues and may cause truncation and rounding errors while approximating the exact solution [21]–[23]. In reality, besides quantitative analyses, researchers also need to consider qualitative analyses of these circuits, which must be guaranteed to be convergent, for deeper theoretical investigation, analysis, and understanding of this novel chaotic system. It is also well known that analytical method enables qualitative analysis and closed-form expression and, thus, guarantees convergence. With analytical method, researchers can predict the performance of memristive circuits and optimize circuit parameters more clearly and conveniently [24]. Moreover, the solutions derived from the analytical method can be easily integrated into Electronic Design Automation (EDA) software for circuit synthesis [25]. Hence, analytical method is crucial for memristive chaotic system.

Although some progresses have been made in this area, at least two major obstacles must be overcome as far as the authors' knowledge:

1) The research using analytical method to analyze chaotic circuit is still in its infancy.
2) The adopted methods in these studies scarcely perform accuracy and convergence optimizations for the obtained solution.

It is known *Homotopy* [26] is an efficient analytical method of linearizing the original nonlinear equation to solve a nonlinear problem. It has been commonly used in memristor modeling [25], [27]. For instance, Hernández-Mejía *et al.* [25] developed an analytical modeling method for HP memristor [4] using *Homotopy Perturbation Method* (HPM) and applied it in a memristive amplifier. Unfortunately, the amplifier is not chaotic; Vazquez-Leal *et al.* [28] successfully adopted *Multistage Homotopy Perturbation Method* (MuHPM) [29] to obtain the analytical approximate solutions of chaotic trajectories in memristive circuit. However, the work in [25] and [29] are all based on HPM [30]–[32] that is essentially a perturbation method [33], [34], and hence has the same limitations as the perturbation method, e.g., HPM and MuHPM cannot always guarantee the fast convergence of solution, which may lead to the poor approximation accuracy [33], [35]. Here, ''approximation accuracy'' is defined as the error between a solved solution and an exact solution (if it exists) that is generally hard to derive due to memristor's complex physical equation. On the other hand, for memristive chaotic circuits, their circuit classifications, device parameters, and memristor models are quite different from each other. For these reasons, researchers need a scalable analytical method capable of optimizing accuracy of the solved solution depending on different applications.

To address the aforementioned limitations, inspired by the remarkable works in [25] and [29], we propose a novel analytical method combining *Multi-objective Optimization* (MO) and *Homotopy Analysis Method* (HAM), called MO-MIHAM that has the following advantages:

1) It enables both qualitative and quantitative analyses and high freedom to choose homotopy-related terms, and it is insensitive to convergence issues.
2) It can be easily integrated into EDA software for circuit synthesis and has high scalability.
3) It can provide a reasonable tradeoff between approximation accuracy, computational complexity and execution time.
4) It is characterized by higher approximation accuracy and computational performance (comprehensively considering the accuracy, computational complexity and execution time), compared with the traditional homotopy-based analytical methods listed in this paper.

In our proposed method, the traditional HAM convergence control parameters in *homotopy deformation equations* that are constructed for solving unknown variables (chaotic trajectories) in ODEs describing memristive circuit, are divided into lots of subintervals in time domain and then optimized by MO for better convergence and accuracy (our method is accordingly named by MO-MIHAM). This idea is based on the fact that convergence control parameter $\hbar$ is a key parameter employed in HAM for accelerating convergence and achieving high accuracy of solution [36], [37], thus optimized $\hbar$ corresponds to optimized convergence and accuracy. To realize this, one of the commonly used MO method—*Technique for Order Preference by Similarity to an Ideal Solution* (TOPSIS) [38], is chosen for $\hbar$ optimization because of its high flexibility and simplicity [39]. In this paper, we accurately tracked the chaotic trajectories, i.e., obtained the analytical approximate solutions of variables, in classical Memristor-Capacitor-Inductor (MCL) and current memristive Band Pass Filter (BPF) chaotic circuits with different types of memristor, by first defining the MO-MIHAM. Note that all the solution procedures and comparisons in this paper were implemented by *Mathematica* 11.2 [40] simulations.

The paper is organized as follows. In Section II the basic solution procedure of MO-MIHAM is introduced. As examples of specific solution procedure, in Section III we obtain the analytical approximate solutions of unknown variables in MCL circuit and memristive BPF chaotic circuit, respectively. Then these solved analytical solutions are verified and compared with solutions obtained from HPM, HAM, MuHPM, and RKF45-based numerical analysis, in Section IV. Some discussions are given in Section V. Finally, in Section VI, the conclusion is summarized.

II. MO-MIHAM SOLUTION PROCEDURE

The HAM [35], [36], [41]–[43], which is essentially based on the *Homotopy* [26] in the *Topology* [44], is an approximate

methodology to obtain the explicit form solution of ODE. Overall, it can be viewed as a method of linearizing the original ODE to solve a nonlinear problem. HAM was firstly proposed by Liao [41]. Since then, it has been extensively explored in various areas [45]–[48].

In the frame of MO-MIHAM, which is based on the HAM, the r-th equation in ODEs that describes a dynamic system has the following expression:

$$\mathscr{N}_r\left[u_1(t),\ldots,u_r(t),\ldots,u_R(t)\right]=0, \tag{1}$$

where $\mathscr{N}_r$ represents a nonlinear operator, $u_1(t)$, $u_r(t)$, and $u_R(t)$ denote the first, r-th ($r\in[1,R]$, $r\in\mathbb{N}$), and R-th variables that needed to be analytically solved, R is the number of equations and variables respectively, t is time variable.

With (1), the ODEs regarding a dynamic system can be expressed by

$$\begin{cases}\mathscr{N}_1\left[u_1(t),\ldots,u_r(t),\ldots,u_R(t)\right]=0\\ \vdots\\ \mathscr{N}_r\left[u_1(t),\ldots,u_r(t),\ldots,u_R(t)\right]=0\\ \vdots\\ \mathscr{N}_R\left[u_1(t),\ldots,u_r(t),\ldots,u_R(t)\right]=0.\end{cases} \tag{2}$$

Let us suppose the time span of (2) is $I=[t_0,T]$, where t_0 is the initial time and T is the final time. Then, we divide I into S subintervals, i.e., $[t_0,t_1),[t_1,t_2),\ldots[t_{i-1},t_i),\ \ldots\ [t_{S-1},t_S=T]$. The i-th ($i\in[1,S]$, $i\in\mathbb{N}$) subinterval is described by $I_i=[t_{i-1},t_i]$, where $i=1,2,\ldots,S, i\in\mathbb{N}$. The time step size and initial time in I_i is $\Delta t=t_i-t_{i-1}=(T-t_0)/S$ and $t_{i,0}=t_0+\Delta t\times(i-1)$, respectively.

Because of the division of time t mentioned above, $u_r(t)$ in (1) is correspondingly divided into S subintervals in regard to t

$$u_r(t)=\sum_{i=1}^{S}u_{i,r}(t), \tag{3}$$

where $u_{i,r}(t)$ is the exact solution (assuming it exists) of $u_r(t)$ in I_i, $r\in[1,R]$, $i\in[1,S]$.

Then, we construct the *zero-order homotopy deformation equations* in I_i to solve (2) as shown in (4), as shown at the top of the next page, where $t\in I_i$ and $r\in[1,R]$, i.e., (4) represent R equations from $r=1$ to $r=R$. $\phi_{i,r}(t;q)$ denotes the r-th unknown function needed to be solved to approximate the $u_{i,r}(t)$, the embedded parameter $q\in[0,1]$, $\hbar_{i,r}\in\mathbb{R}^-$ is a introduced convergence control parameter, which is a key parameter used in MO-MIHAM for accelerating the convergence of approximation, $H_{i,r}(t)\neq 0$ denotes an auxiliary functions in I_i, $u_{i,r,0}(t)$ is an initial value of $u_{i,r}(t)$ in I_i, and $\mathscr{L}_r$ represents an auxiliary linear operator depending on the chosen base function (generally, exponential, polynomial, Fourier, and Chebyshev functions are adopted [32]), on which the characteristics of (1) is based. Note that $r\in[1,R]$ and $i\in[1,S]$ in the above parameter explanations.

In (4), original ODE is linearized by $\mathscr{L}_r$, which is a typical feature of homotopy *Homotopy* [35], [42]. That is, we establish a relationship between $\phi_{i,r}(t;q)$ and $u_{i,r}(t)$ by using homotopy transition in (4). It is known one of the advantages of HAM is the high freedom to choose homotopy-related terms (i.e., $\hbar$, $H(t)$, and $\mathscr{L}$) in *zero-order homotopy deformation equation* [35], [42], terms in MO-MIHAM (i.e., $\hbar_{i,r}$, $H_{i,r}(t)$, and $\mathscr{L}_r$) inherits this advantage by constructing (4).

For the initial value $u_{i,r,0}(t)$ of subinterval I_i,

$$u_{i,r,0}(t)=\begin{cases}u_{r,0} & i=1\\ u_{i-1,r,N}\left[t_0+\Delta t\times(i-1)\right] & i>1,\end{cases} \tag{5}$$

where $u_{r,0}$ is the given initial value of $u_r(t)$ for I.

Clearly, when respectively substituting $q=0$ and $q=1$ into (4) and comparing the obtained equations with (1) and (3), they hold

$$\phi_{i,r}(t;0)=u_{i,r,0}(t), \tag{6}$$

$$\left\{\phi_{i,1}(t;1),\ldots,\phi_{i,r}(t;1),\ldots,\phi_{i,R}(t;1)\right\}=\{u_{i,1}(t),\ldots,u_{i,r}(t),\ldots,u_{i,R}(t)\}. \tag{7}$$

Therefore, we have a conclusion from (6) and (7) that, as q changes from 0 to 1, $\phi_{i,r}(t;q)$ is transited from the initial value $u_{i,r,0}(t)$ to exact solution $u_{i,r}(t)$, which is also a typical feature of *Homotopy* [35], [42].

Assuming $\phi_{i,r}(t;q)$ is a continuously smooth function regarding to q and considering (6), $\phi_{i,r}(t;q)$ can be expanded into a *Maclaurin-series* relative to q ($q\in[0,1]$)

$$\phi_{i,r}(t;q)=u_{i,r,0}(t)+\sum_{m=1}^{+\infty}u_{i,r,m}(t)\,q^m, \tag{8}$$

where m denotes the number of approximation order, and

$$u_{i,r,m}(t)=\mathscr{D}_m[\phi_{i,r}(t;q)], \tag{9}$$

$$\mathscr{D}_m=\frac{1}{m!}\frac{\partial^m}{\partial q^m}|_{q=0}, \tag{10}$$

in which terms $u_{i,r,m}(t)$ in (8) and (9) are defined as the mth-order *homotopy coefficient*, which cannot be solved from (9) and (10) because $\phi_{i,r}(t;q)$ in (9) is unknown, they are determined by the *high-order homotopy deformation equations* presented later, $\mathscr{D}_m$ is defined as the mth-order *homotopy derivative operator*.

When $q=1$, according to (5), (7), and (8), we have

$$\phi_{i,r}(t;1)=u_{i,r}(t)=u_{i,r,0}(t)+\sum_{m=1}^{+\infty}u_{i,r,m}(t). \tag{11}$$

From the homotopy point of view [41]–[43], (11) is called the analytical *homotopy series solution* and is one of the solutions of $u_{i,r}(t)$.

It is should be noted that (11) can be solved, as long as $\hbar_{i,r}$, $H_{i,r}(t)$, and $\mathscr{L}$ are properly chosen (the choices of $\hbar_{i,r}$, $H_{i,r}(t)$ and $\mathscr{L}$ shall be explained later in Section II and Section III, respectively) to guarantee the following preconditions:

$$(1-q)\mathscr{L}_r\left[\phi_{i,r}(t;q)-u_{i,r,0}(t)\right]=-q\hbar_{i,r}H_{i,r}(t)\mathscr{N}_r\left[\phi_{i,1}(t;q),\ldots,\phi_{i,r}(t;q),\ldots,\phi_{i,R}(t;q)\right] \tag{4}$$

1) The solution $\phi_{i,r}(t;q)$ of the *zero-order deformation equation* (4) exists for all $q\in[0,1]$;
2) The *Maclaurin-series* (8) of $\phi_{i,r}(t;q)$ converges at $q=1$;
3) The deformation derivative (9) exists for $m=1,2,\ldots,+\infty, m\in\mathsf{N}$.

Differentiating (4) m times in regard to q and setting $q=0$, then dividing both sides of the obtained expression by $m!$, the *high-order homotopy deformation equations* is obtained as shown in (12), as shown at the bottom of the next page, to solve terms $u_{i,r,m}(t)$ in (11), where

$$\chi_m=\begin{cases}0 & m=1\\ 1 & m>1,\end{cases} \tag{13}$$

and (12) represent R equations from $r=1$ to $r=R$.

According to (8) and (9), the $(m-1)$th-order *homotopy derivative* $\mathscr{D}_{m-1}\left\{\mathscr{N}_r\left[\phi_{i,1}(t;q),\ldots,\phi_{i,r}(t;q),\ldots,\phi_{i,R}(t;q)\right]\right\}$ in (12) is dependent upon $u_{i,r,0}(t), u_{i,r,1}(t),\ldots,u_{i,r,m-1}(t)$. Therefore, we can obtain $u_{i,r,1}(t), u_{i,r,2}(t),\ldots,u_{i,r,m}(t)$ by respectively performing the operations of inverse linear operators $\mathscr{L}^{-1}=\{\mathscr{L}_1^{-1},\ldots,\mathscr{L}_r^{-1},\ldots,\mathscr{L}_R^{-1}\}$ on both sides of (12) and performing *homotopy derivative* one after the other in order. Since this step is closely related to the specific choice of $\mathscr{L}^{-1}=\{\mathscr{L}_1,\ldots,\mathscr{L}_r,\ldots,\mathscr{L}_R\}$, the detailed solution procedure shall be illustrated in Section III, where ODEs describing MCL circuit is employed as a case study.

After combining (7), (11), and (12), and then considering the unknown convergence control parameters vector $\hbar_i=\left\{\hbar_{i,1},\ldots,\hbar_{i,r},\ldots,\hbar_{i,R}\right\}$, we deduce the N-order analytical approximate solution [truncated *homotopy series solution* of (11)] $u_{i,r,N}(t,\hbar_i)$ of $u_{i,r}(t)$

$$u_{i,r}(t)=u_{i,r,N}(t,\hbar_i)=u_{i,r,0}(t)+\sum_{m=1}^{N}u_{i,r,m}(t,\hbar_i), \tag{14}$$

where N denotes the final approximation order, the mth-order analytical approximate expression of $u_{i,r,m}(t,\hbar_i)$ can be solved by performing the operations of inverse linear operators $\mathscr{L}^{-1}$ on both sides of (12), the $u_{i,r,m-1}(t)$ and $\mathscr{D}_{m-1}$ terms in (12) are derived from (9) and (10), and $u_{i,r,0}(t)$ is from (5). Note that besides $u_r(t)$, the original r-th ODE includes other variables $\{u_1(t),\ldots,u_r(t),\ldots,u_R(t)\}$, $\mathscr{N}_r$ terms in (4) and (12) are therefore dependent upon other corresponding approximation functions $\{\phi_{i,1}(t;q),\ldots,\phi_{i,r}(t;q),\ldots,\phi_{i,R}(t;q)\}$ and, thus, upon $\hbar_i=\{\hbar_{i,1},\ldots,\hbar_{i,r},\ldots,\hbar_{i,R}\}$, this is because in subinterval, each ϕ corresponds to each $\hbar$.

With above analyses, we know $\hbar_i$ significantly affects the convergence and accuracy of (14) derived from (12) (before (14), we suppose $\hbar_{i,r}$ in $\hbar_i$ is properly chosen for simplicity), like $\hbar$ in HAM. Because of this, solving the optimized $\hbar_i$ is a crucial step in MO-MIHAM to obtain the complete solution of (14) with high accuracy. After obtaining the R incomplete solutions of variables in I_i by repeatedly performing (14) for changing r from 1 to R ('incomplete' here refers to elements in $\hbar_i$ needed to be solved later), $\hbar_i$ can be solved (optimized) by synchronously minimizing the *discrete squared residual errors* [37] of (2) as follows:

$$\begin{cases}E_{i,1,N}(\hbar_i)\\ \quad\vdots\\ E_{i,r,N}(\hbar_i)\\ \quad\vdots\\ E_{i,R,N}(\hbar_i),\end{cases} \tag{15}$$

where the *discrete squared residual error* of (1) is based on (14) and has the following expression:

$$E_{i,r,N}(\hbar_i)\approx\frac{1}{N_P+1}\sum_{p=\mathbf{1}}^{N_P}\left\{\mathscr{N}_r\left[\sum_{m=1}^{N}u_{i,r,0}(t)+u_{i,r,m}\left(t_p,\hbar_i\right)\right]\right\}^2, \tag{16}$$

in which N_P is the number of time points uniformly chosen for calculating $E_{i,r,N}(\hbar_i)$, $t_{p,i}=t_{i-1,0}+p\Delta t'$ is the p-th time point in I_i, and

$$\Delta t'=\frac{\Delta t}{N_P}. \tag{17}$$

It should be emphasized that solving minimum (15) is essentially a *Multi-objective optimization* (MO). Considering its high flexibility and simplicity, the TOPSIS method [38] is adopted to minimize (15) for obtaining $\hbar_i$ as follows:

$$\begin{aligned}&min\sqrt{\sum_{r=1}^{R}\lambda_r\left|E_{i,r,N}(\hbar_i)-E_{i,r,N}\left(\hbar_i^*\right)\right|^2}\rightarrow\hbar_i,\\ &s.t.\,\hbar_{i,r}\in\mathbb{R}^-,\hbar_{i,r}^*\in\mathbb{R}^-,\end{aligned} \tag{18}$$

where λ_r is the weight coefficient of r-th equation in (2), $E_{i,r,N}\left(\hbar_i^*\right)$ is the optimal value of $E_{i,r,N}(\hbar_i)$, $\hbar_i^*=\{\hbar_{i,1}^*,\ldots,\hbar_{i,r}^*,\ldots,\hbar_{i,R}^*\}$ is derived from the signal-objective function optimization of $E_{i,r,N}(\hbar_i)$.

Generally, the faster elements in $\hbar_i$ approach to their optimal values that correspond to the minimum (15), the faster $u_{i,r,N}(t,\hbar_i)$ converges to the exact solution $u_{i,r}(t)$ of original ODE (1) in I_i, hence indicating higher approximation accuracy [35]. It is well known that there may be not a solution in the MO procedure that satisfies all constraints and enables all objective functions to be globally optimal at the same time. Therefore, the solution of the MO problem is not unique, but non-inferior [49], [50]. Accordingly, the solved $\hbar_i$ and minimum (15) are non-inferior solution sets, and hence the approximation accuracy is also non-inferior. In spite

of these non-inferior characteristics, MO-MIHAM still has higher accuracy, compared with traditional homotopy-based analytical methods without using MO, which shall be shown in Section IV.

Then, substituting the obtained $\hbar_i$ into (14), we have the complete N-order analytical approximate solution $u_{i,r,N}(t)$ in I_i. Finally, repeating same solution procedures from $i = 1$ to $i = S$, we obtain N-order analytical approximate solution $u_{S,r,N}(t)$ of variable $u_r(t)$ in I

$$u_r(t) = u_{S,r,N}(t) = \sum_{i=1}^{S} \chi[I_i] u_{i,r,N}(t), \tag{19}$$

which satisfies the original equation (1), and

$$\chi[I_i] = \begin{cases} 1 & t \in I_i \\ 0 & t \notin I_i. \end{cases} \tag{20}$$

For other variables in original ODEs (2), repeatedly performing the solution procedures, similar to those for $u_r(t)$, from $r = 1$ to $r = R$, we have their complete N-order analytical approximate solution sets for the time span I as follows:

$$\{u_1(t), \ldots, u_r(t), \ldots, u_R(t)\} = \left\{u_{S,1,N}(t), \ldots, u_{S,r,N}(t), \ldots, u_{S,R,N}(t)\right\}. \tag{21}$$

In Algorithm 1, we summarize the core procedure mentioned before to account for MO-MIHAM more clearly and systematically. The application and specific solution procedure for MO-MIHAM shall be shown in Section III.

Algorithm 1 Solution Procedure of MO-MIHAM for Analytically Solving $u_r(t)$ in ODEs (2), $r \in [1, R]$, $r \in \mathbb{N}$.

1 Determine the approximation order N and base function;
2 Divide the time span I into S subintervals;
3 ***for*** *i-th time subinterval* I_i, $i = 1$, ***do***
4 Choose the auxiliary function $H_{i,r}(t)$ and the linear operator $\mathscr{L}_r$, and give the initial value $u_{r,0}$;
5 Construct zero-order deformation equations (4) and corresponding m th-order deformation equations (12) of variable $u_{i,r}(t)$ based on the original ODEs (2);
6 Determine the initial value $u_{i,r,0}(t)$, (5);
7 ***for*** $m = 1$, ***do***
8 Solve mth-order deformation equation (12), $t \in I_i$;
9 $m = m + 1$;
10 ***if*** $m > N$, ***then***
11 Stop the iteration, let $m = N$, and solve $u_{i,r,N}(t, \hbar_i)$, $\hbar_i = \left\{\hbar_{i,1}, \ldots, \hbar_{i,r}, \ldots, \hbar_{i,R}\right\}$;
12 ***end if***
13 ***end for***
14 Minimizing the discrete squared residual errors by MO (e.g., TOPSIS) to solve $\hbar_i$ and $u_{i,r,N}(t)$, $u_{i,r,N}(t, \hbar_i) \overset{(15)(18)}{\longrightarrow} \hbar_i \overset{(14)}{\longrightarrow} u_{i,r,N}(t)$;
15 $i = i + 1$;
16 ***if*** $i > S$, ***then***
17 Stop the iteration, let $i = S$, obtain solution $u_r(t) = u_{S,r,N}(t) = \sum_{i=1}^{S} \chi[I_i] u_{i,r,N}(t)$, $r \in [1, R]$, (19) and (20);
18 ***end if***
19 ***end for***
20 ***end***

III. APPLICATION OF MO-MIHAM IN MEMRISTIVE CHAOTIC CIRCUITS

A. MCL CIRCUIT

For the purpose of verifying the effectiveness of the proposed MO-MIHAM method, the classical MCL-based chaotic circuit [51] was used, as a case study for the application of MO-MIHAM to trace the chaotic trajectories. Fig. 1 shows the MCL circuit. It is a three-element circuit composed of a capacitor C, an inductor L, and a memristor M. According to the Kirchhoff's Current and Voltage Laws and nonlinear characteristic of the memristor, the dynamics behavior of MCL circuit can be described by a set of ODEs

$$\begin{cases} dV(t)/dt = I/Cap \\ dI(t)/dt = -[V + I\beta(SV^2 - 1)]/Lind \\ dSV(t)/dt = -I - \alpha SV + I \cdot SV, \end{cases} \tag{22}$$

where $V(t)$ is the voltage across the capacitor, $I(t)$ is the loop current, $SV(t)$ is the core parameter of memristor—state variable, α and β are the dynamics parameters of memristor M, Cap is the capacitance of C and $Lind$ is the inductance of L. The mathematical model of M is [50]: $V(t) = \beta\left(SV^2 - 1\right) I(t)$, $dSV(t)/dt = I(t) - \alpha SV(t) - SV(t) I(t)$, hence M is a current-controlled memristor defined by Chua in [52]. It is clear from Fig. 1 and (22) that, there are three variables needed to be solved, i.e., $V(t)$, $I(t)$, and $SV(t)$, and MCL circuit is an autonomous continuous-time chaotic system. All the parameters of devices in MCL circuit and the simulation parameters are summarized in Table 1.

In the following Section III. A, we show how to track dynamical trajectories of MCL circuit by using MO-MIHAM. Note that for the simpler notation, we define $x = V(t)$, $y = I(t)$, $z = SV(t)$, and $\left\{u_{i,1,m}(t), u_{i,2,m}(t), u_{i,3,m}(t)\right\} = \left\{x_{i,m}(t), y_{i,m}(t), z_{i,m}(t)\right\}$.

Firstly, according to the expression characteristics of (22), i.e., each equation in (22) is a first-order ODE, we choose the

$$\mathscr{L}_r\left[u_{i,r,m}(t) - \chi_m u_{i,r,m-1}(t)\right] = \hbar_{i,r} H_{i,r}(t)\, \mathscr{D}_{m-1}\left\{\mathscr{N}_r\left[\phi_{i,1}(t; q), \ldots, \phi_{i,r}(t; q), \ldots, \phi_{i,R}(t; q)\right]\right\} \tag{12}$$

TABLE 1. Dynamics parameters of memristor M, devices parameters of C and L in MCL circuit (Fig. 1), and simulation parameters.

Parameter	Value	Unit	Definition
Cap[a]	1	F	Capacitance of C
$Lind$[a]	3.3	H	Inductance of L
$V(0)$[a]	0.1	V	Initial voltage $V(t)$ across C
$I(0)$[a]	0.1	A	Initial loop current $I(t)$
$SV(0)$[a]	0	--	Initial state variable $SV(t)$ of memristor
α[a]	0.2	--	Dynamics parameter of memristor
β[a]	1.7	--	Dynamics parameter of memristor
t_0	0	s	Initial time of MCL circuit
Δt	0.1	s	Time step size of subintervals, $\Delta t = I/S$
N_P	100	--	Number of time points chosen for calculating $E_{i,r,N}$ in I_i
R	3	--	Total number of ODE and variables in MCL dynamic system
S	1000	--	Total number of subintervals in I
N	4	--	Final approximation order

[a] The parameter is obtained from [51].

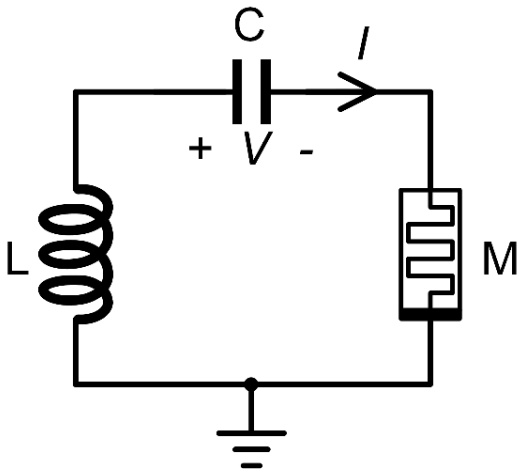

FIGURE 1. MCL circuit.

following polynomial as base function

$$\left\{t^n \middle| n = 1, 2, 3, \ldots\right\}. \tag{23}$$

Therefore, the solutions of three variables in MCL circuit in subinterval I_i can be expressed by

$$u_{i,r}(t) = \sum_{n=0}^{+\infty} a_{r,n} t^n, \tag{24}$$

where $a_{r,n}$ is the polynomial coefficients needed to be solved later. Note that $u_{i,r}(t)$ represents the three variables and hence (24) represents three equations from $r = 1$ to $r = 3$.

Based on (22) and (23), we choose every auxiliary linear operator in (4) as first-order differential operator ($r \in [1,R]$, $R = 3$ for MCL circuit)

$$\mathscr{L}_r[\phi(t;q)] = \mathscr{L}[\phi(t;q)] = \frac{\partial \phi(t;q)}{\partial t}, \tag{25}$$

with the property

$$\mathscr{L}_r[C] = \mathscr{L}[C] = 0, \tag{26}$$

where C is a constant.

Then, on the basis of (4) and (22), the *zero-order homotopy deformation equations* in I_i are constructed as (27), as shown at the top of the next page, where $x_{i,0}(t) = V(0)$, $y_{i,0}(t) = I(0)$, and $z_{i,0}(t) = SV(0)$ according to Table 1, $\{x_i(t;q), y_i(t;q), z_i(t;q)\}$ is equal to $\{\phi_{i,1}(t;q), \phi_{i,2}(t;q), \phi_{i,3}(t;q)\}$ in (4) and the related nonlinear operators for (22) in I_i are given by (28), as shown at the top of the next page.

Like (6), when $q = 0$, we have

$$\begin{aligned} &x_i(t;0) = x_{i,0}(t), \quad y_i(t;0) = y_{i,0}(t), \\ &z_i(t;0) = z_{i,0}(t), \end{aligned} \tag{29}$$

and like (7), when $q = 1$, we have

$$x_i(t;1) = x_i(t), \quad y_i(t;1) = y_i(t), \quad z_i(t;1) = z_i(t). \tag{30}$$

Expanding $x_i(t;q)$, $y_i(t;q)$, and $z_i(t;q)$ into three *Maclaurin-series* in regards to q (it is known $q \in [0, 1]$)

$$\begin{cases} x_i(t;q) = x_{i,0}(t) + \sum_{m=1}^{+\infty} x_{i,m}(t)\, q^m \\ y_i(t;q) = y_{i,0}(t) + \sum_{m=1}^{+\infty} y_{i,m}(t)\, q^m \\ z_i(t;q) = z_{i,0}(t) + \sum_{m=1}^{+\infty} z_{i,m}(t)\, q^m, \end{cases} \tag{31}$$

in which $x_{i,m}(t)$, $y_{i,m}(t)$, and $z_{i,m}(t)$ are solved by *high-order homotopy deformation equations* described later.

From (30) and (31), we have the following homotopy series solutions when $q = 1$, like (11):

$$\begin{cases} x_i(t) = x_{i,0}(t) + \sum_{m=1}^{+\infty} x_{i,m}(t) \\ y_i(t) = y_{i,0}(t) + \sum_{m=1}^{+\infty} y_{i,m}(t) \\ z_i(t) = z_{i,0}(t) + \sum_{m=1}^{+\infty} z_{i,m}(t). \end{cases} \tag{32}$$

Then, the *high-order homotopy deformation equations* (33), as shown at the top of the next page, are obtained from (12) and (28) to solve (32). After performing the operations of inverse linear operator $\mathscr{L}^{-1}$ [i.e., integration with t, based on $\mathscr{L}$ from (29)] on both sides of (33), and then rearranging the related equations, the solutions of the mth-order deformation equations (33) becomes (34), as shown at the top of the next page, where the integral constant C_1, C_2, and C_3 are determined by $x_{i,0}(t)$, $y_{i,0}(t)$, and $z_{i,0}(t)$. The auxiliary functions $H_{i,1}(t)$, $H_{i,2}(t)$, and $H_{i,3}(t)$ are all set to 1, which is commonly used for simplicity and for following the *rule of regularity of solutions* in HAM [35]. With (28) and (m-1)th-order *homotopy derivative operator* $\mathscr{D}_{m-1}$ derived from (10), we have (35), as shown at the top of the next page. Substituting (35) into (34), then

$$\begin{cases} (1-q)\,\mathscr{L}\left[x_i(t;q)-x_{i,0}(t)\right]=-q\hbar_{i,1}H_{i,1}(t)\,\mathscr{N}_1\left[y_i(t;q)\right] \\ (1-q)\,\mathscr{L}\left[y_i(t;q)-y_{i,0}(t)\right]=-q\hbar_{i,2}H_{i,2}(t)\,\mathscr{N}_2\left[x_i(t;q),y_i(t;q),z_i(t;q)\right] \\ (1-q)\,\mathscr{L}\left[z_i(t;q)-z_{i,0}(t)\right]=-q\hbar_{i,3}H_{i,3}(t)\,\mathscr{N}_3\left[y_i(t;q),z_i(t;q)\right], \end{cases} \tag{27}$$

$$\begin{cases} \mathscr{N}_1\left[y_i(t;q)\right]=dV(t)/dt-y_i(t;q)/Cap \\ \mathscr{N}_2\left[x_i(t;q),y_i(t;q),z_i(t;q)\right]=dI(t)/dt+\dfrac{\left[x_i(t;q)+\beta y_i(t;q)\left(z_i(t;q)^2-1\right)\right]}{Lind} \\ \mathscr{N}_3\left[y_i(t;q),z_i(t;q)\right]=dSV(t)/dt+y_i(t;q)+\alpha z_i(t;q)-y_i(t;q)\,z_i(t;q), \end{cases} \tag{28}$$

$$\begin{cases} \mathscr{L}\left[x_{i,m}(t)-\chi_m x_{i,m-1}(t)\right]=\hbar_{i,1}H_{i,1}(t)\,\mathscr{D}_{m-1}\{\mathscr{N}_1\left[y_i(t;q)\right]\} \\ \mathscr{L}\left[y_{i,m}(t)-\chi_m y_{i,m-1}(t)\right]=\hbar_{i,2}H_{i,2}(t)\,\mathscr{D}_{m-1}\{\mathscr{N}_2\left[x_i(t;q),y_i(t;q),z_i(t;q)\right]\} \\ \mathscr{L}\left[z_{i,m}(t)-\chi_m z_{i,m-1}(t)\right]=\hbar_{i,3}H_{i,3}(t)\,\mathscr{D}_{m-1}\{\mathscr{N}_3\left[y_i(t;q),z_i(t;q)\right]\}. \end{cases} \tag{33}$$

$$\begin{cases} x_{i,m}(t)=\hbar_{i,1}\int_0^t H_{i,1}(\tau)\,\mathscr{D}_{m-1}\{\mathscr{N}_1\left[y_i(\tau;q)\right]\}d\tau+\chi_m x_{i,m-1}(t)+C_1 \\ y_{i,m}(t)=\hbar_{i,2}\int_0^t H_{i,2}(\tau)\,\mathscr{D}_{m-1}\{\mathscr{N}_2\left[x_i(\tau;q),y_i(\tau;q),z_i(\tau;q)\right]\}d\tau+\chi_m y_{i,m-1}(t)+C_2 \\ z_{i,m}(t)=\hbar_{i,3}\int_0^t H_{i,3}(\tau)\,\mathscr{D}_{m-1}\{\mathscr{N}_3\left[y_i(\tau;q),z_i(\tau;q)\right]\}d\tau+\chi_m z_{i,m-1}(t)+C_3. \end{cases} \tag{34}$$

$$\begin{cases} \mathscr{D}_{m-1}\{\mathscr{N}_1\left[y_i(t;q)\right]\}=dx_{i,m-1}(t)/dt-y_{i,m-1}(t)/Cap \\ \mathscr{D}_{m-1}\{\mathscr{N}_2\left[x_i(t;q),y_i(t;q),z_i(t;q)\right]\}=\dfrac{dy_{i,m-1}(t)}{dt}+\dfrac{x_{i,m-1}(t)+\beta\sum_{n=0}^{m-1}\sum_{j=0}^{n}z_{i,m-1-n}(t)\,z_{i,n-j}(t)y_{i,j}(t)-\beta y_{i,m-1}(t)}{Lind} \\ \mathscr{D}_{m-1}\{\mathscr{N}_3\left[y_i(t;q),z_i(t;q)\right]\}=dy_{i,m-1}(t)/dt+y_{i,m-1}(t)+\alpha z_{i,m-1}(t)-\sum_{n=0}^{m-1}y_{i,n}(t)z_{i,m-1-n}(t). \end{cases} \tag{35}$$

considering (32) and unknown convergence control parameters vector $\hbar_i=\{\hbar_{i,1},\hbar_{i,2},\hbar_{i,3}\}$, the incomplete N-order analytical approximate solutions of three variables in subinterval I_i, like (14), can be obtained:

$$\begin{cases} x_i(t)=x_{i,N}(t,\hbar_i)=x_{i,0}(t)+\sum_{m=1}^{N}x_{i,m}(t,\hbar_i) \\ y_i(t)=y_{i,N}(t,\hbar_i)=y_{i,0}(t)+\sum_{m=1}^{N}y_{i,m}(t,\hbar_i) \\ z_i(t)=z_{i,N}(t,\hbar_i)=z_{i,0}(t)+\sum_{m=1}^{N}z_{i,m}(t,\hbar_i). \end{cases} \tag{36}$$

Finally, after solving $\hbar_i$ through TOPSIS based MO (16)–(18) with $\lambda_r=1$ and substituting the solved $\hbar_i$ into (36), we derive the complete N-order analytical approximate solutions of three variables in the time span I (S subintervals) as follows [based on (19)–(21)]:

$$\begin{cases} x(t)=x_{S,N}(t)=\sum_{i=1}^{S}\chi\left[I_i\right]x_{i,N}(t) \\ y(t)=y_{S,N}(t)=\sum_{i=1}^{S}\chi\left[I_i\right]y_{i,N}(t) \\ z(t)=z_{S,N}(t)=\sum_{i=1}^{S}\chi[I_i]z_{i,N}(t), \end{cases} \tag{37}$$

where $\chi[I_i]=\begin{cases}1 & t\in I_i\\ 0 & t\notin I_i\end{cases}$.

For the purpose of showing the above procedure more clearly, the solved solution expressions of the first two subintervals (i.e., $i=1$ and 2) of $x_{i,N}(t)$, $y_{i,N}(t)$, and $z_{i,N}(t)$, are shown as examples in the Appendix.

B. MEMRISTIVE BAND PASS FILTER CHAOTIC CIRCUIT

In this subsection, MO-MIHAM is applied in the recently proposed memristive Band Pass Filter (BPF) chaotic circuit [6], i.e., BPF's chaotic dynamics are analytically analyzed by using MO-MIHAM, for the purpose of demonstrating the wide applicability of MO-MIHAM.

Fig. 2 shows the BPF chaotic circuit, which is a third-order nonlinear circuit composed of one memristor M, one amplifier U, two capacitors C_1 and C_2, and three resistors R_1–R_3. ODEs (38) describe the dynamic behavior of BPF circuit, in which δ is a dynamics control parameter, $k=1+R_2/R_3$, $C_1=C_2=C$. Note that device parameters of BPF in Fig. 2 are all scaled in a dimensionless form. The system parameters $\rho=80$, $\varepsilon=50/3$, $g=0.1$, and $k=21$ are taken from [6], except the dynamics control parameter $\delta=R_1C/R_2$ that shall be used in next section for controlling various dynamic behaviors of BPF circuit. From (38), we know the memristive BPF circuit has three unknown physical variables needed to be solved, one is $SV(t)$ denoting the state variable of memristor M, and the others are $V_1(t)$ and $V_2(t)$ representing the two node voltages as shown in Fig. 2.

The ODEs of the memristive BPF was solved by adopting the same solution procedure for MCL circuit, namely, we derived analytic approximate solutions of three variables

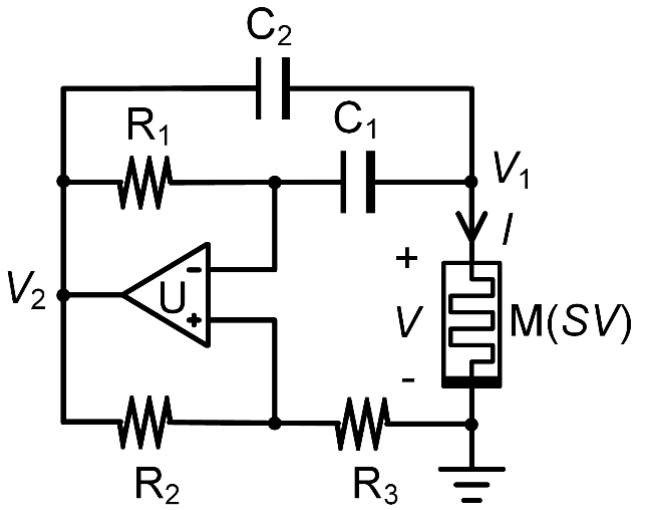

FIGURE 2. Memristive Band Pass Filter chaotic circuit.

by using TO-MIHAM. These solutions shall be shown in the next section.

$$\begin{cases} \dfrac{dSV(t)}{dt} = -\delta SV - \rho V_1 \\ \dfrac{dV_1(t)}{dt} = \varepsilon\left(1 - gSV^2\right) \times V_1/(k-1) - (k+1)\,V_2/k \\ \dfrac{dV_2(t)}{dt} = \varepsilon k\left(1 - gSV^2\right) \times V_1/(k-1) - 2V_2. \end{cases} \tag{38}$$

IV. VERIFICATION AND COMPARISON

A. MCL CIRCUIT

In order to demonstrate the validity and high accuracy of MO-MIHAM, we compared the analytical solutions of three variables obtained in Section III with analytical solutions solved by the traditional homotopy-based methods (i.e., HPM, HAM, and MuHPM), as well as with numerical solutions. Because of high accuracy and wide applicability of the Runge-Kutta-Fehlberg Method (RKF45) [53], [54], we adopted RKF45-based numerical solutions as benchmarks for comparisons. In addition, for the purpose of comparing the error between the analytical solutions and the corresponding numerical solution more clearly, we employed three error parameters for quantitative analysis.

For fairness of the comparisons, the approximate order N and number of subintervals S, in all the homotopy-based methods, were chosen to be 4 and 1000, respectively. The reasons for these choices shall be explained in detail in Section V. B. Considering the complex dynamics evolutions, the time span I was chosen to [0,100]. All the simulation parameters are listed in Table 1.

Figs. 3(a)–3(c) illustrate the evolutions of three variables [i.e., $V(t)$, $I(t)$, and $SV(t)$] solved by MO-MIHAM and RKF45. All the analytical MO-MIHAM solutions accurately track the dynamic trajectories, which is closely in line with RKF45 solutions. To prove the accuracy superiority

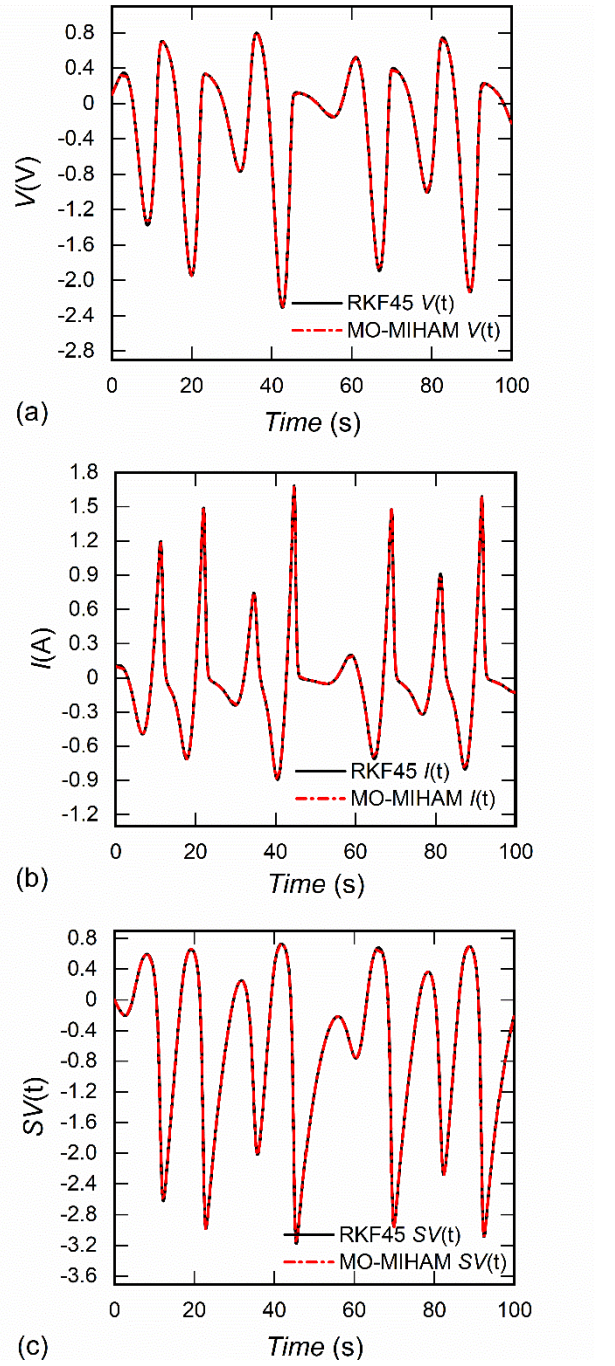

FIGURE 3. Comparisons between the solved three variable in MCL circuit using MO-MIHAM and RKF45-based numerical analysis. (a) Transient trajectory of $V(t)$. (b) Transient trajectory of $I(t)$. (c) Transient trajectory of $SV(t)$.

of MO-MIHAM, we performed quantitative error analyses using three error parameters: *Maximum Relative Error* (*MaxRE*), *Mean Relative Error* (*MRE*), and *Root Mean Square Error* (*RMSE*), i.e., $MaxRE = \max_{1\le k\le N_E} \left|s_n(t_k) - s_a(t_k)/s_n(t_k)\right|$, $MRE = [\sum_{k=1}^{N_E} \left|s_n(t_k) - s_a(t_k)/s_n(t_k)\right|]/N_E$, and $RMSE = \sqrt{\{\sum_{k=1}^{N_E} [s_n(t_k) - s_a(t_k)]^2\}/N_E}$,

TABLE 2. Values of three error parameters for solved $V(t)$ in MCL circuit (See Fig. 1).

Error parameters	HPM4 [25]	HAM4 [35]	MuHPM4 [29]	MO-MIHAM4
MaxRM (%)	5.62042E9	19537.1	2566.25	**919.309**
MRE (%)	1.89013E7	211.118	14.0503	**8.76323**
RMSE	25332.2	0.888210	0.0391420	**0.0181512**

TABLE 3. Values of error parameters for solved $I(t)$.

Error parameters	HPM4 [25]	HAM4 [35]	MuHPM4 [29]	MO-MIHAM4
MaxRM (%)	2.01685E9	13816.5	478.923	**110.371**
MRE (%)	8.80336E6	243.853	13.4484	**8.98204**
RMSE	6837.95	0.473560	0.0316424	**0.0179344**

TABLE 4. Values of error parameters for solved $SV(t)$.

Error parameters	HPM4 [25]	HAM4 [35]	MuHPM4 [29]	MO-MIHAM4
MaxRM (%)	3.28476E8	47760.5	2071.56	**1110.53**
MRE (%)	5.95158E6	430.322	11.8867	**5.60021**
RMSE	29989.3	1.08532	0.0569286	**0.0226105**

where $N_E = N_P \times S$ is the number of time points uniformly chosen in I for error calculations, $t_k = t_0 + kI/N_E$ is the k-th time point, $s_n(t)$ is the RKF45-based numerical solution of $V(t)$, while $s_a(t)$ is the analytical approximate solution of $V(t)$ obtained by the traditional homotopy-based analytical methods or by the newly proposed MO-MIHAM. Tables 2–4 show error parameters for three variables derived from comparisons between solutions solved by the homotopy-based analytical methods (including MO-MIHAM) and RKF45 solutions. From Tables 2–4, we can see clearly the error parameters of MO-MIHAM4 solutions ($N = 4$) are the smallest among all the homotopy-based methods, indicating MO-MIHAM has the highest accuracy under a same approximation order.

Figs. 4(a)–4(c) show the phase portraits of three variables in MCL circuit obtained by MO-MIHAM. These portraits represent typical evolution characteristics of chaotic attractors, also matching the corresponding RKF45 solutions well. Figs. 4(a)–4(c) further demonstrate the characteristics of chaotic attractors in MCL circuit.

In order to further verify the applicability of the proposed method to variations of initial conditions of memristive chaotic circuits, we studied the evolutions of bifurcation diagram of V (voltage across C) and the three Lyapunov exponents (LEs) of the MCL circuit by taking β (the initial dynamic control parameter of the memristor) as a variable, as shown in Fig. 5(a) and 5(b), respectively. As seen from Fig. 5(a), with the increase of β from 1 to 1.8, the evolution of V has a path towards chaos after three period doubling bifurcations. When β is greater than 1.61 (e.g., $\beta = 1.7$ in Figs. 1 and 2), Fig. 5(a) shows a chaotic band composed of

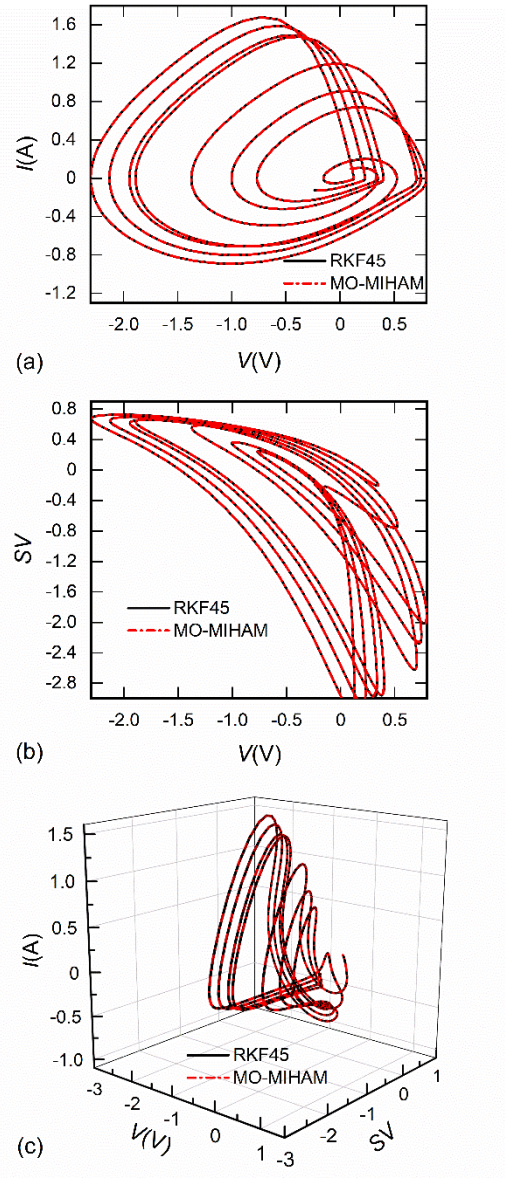

FIGURE 4. Comparisons between the solved phase portraits in MCL circuit by using MO-MIHAM and RKF45-based numerical analysis. (a) Phase portrait in the $V(t)$–$I(t)$ plane. (b) Phase portrait in the $V(t)$–$SV(t)$ plane. (c) 3D phase portrait in the $V(t)$–$SV(t)$–$I(t)$ plane.

disordered discrete points and Fig. 5(b) illustrates the MCL circuit has one positive LE (see LE of V), one nearly zero LE (see LE of I), one negative LE (see LE of SV), and the sum of the three LEs is negative [for $\beta = 1.7$ in Figs. 1 and 2, the LEs are 0.03283, 0.000313, and -0.47107, as seen from Fig. 5(b)]. All these observations indicate the MCL circuit has strange attractors when $\beta > 1.61$. We also have a conclusion from Fig. 5 that, our method is cable of tracking small variations of initial conditions. Therefore, the MCL circuit is chaotic as shown in Figs 3–5, verifying the conclusion in [50].

B. MEMRISTIVE BAND PASS FILTER CHAOTIC CIRCUIT

Figs. 6(a)–6(d) illustrate the dynamic evolutions of phase portraits of memristive BPF circuit (see Fig. 2) in V_1–V_2 plane.

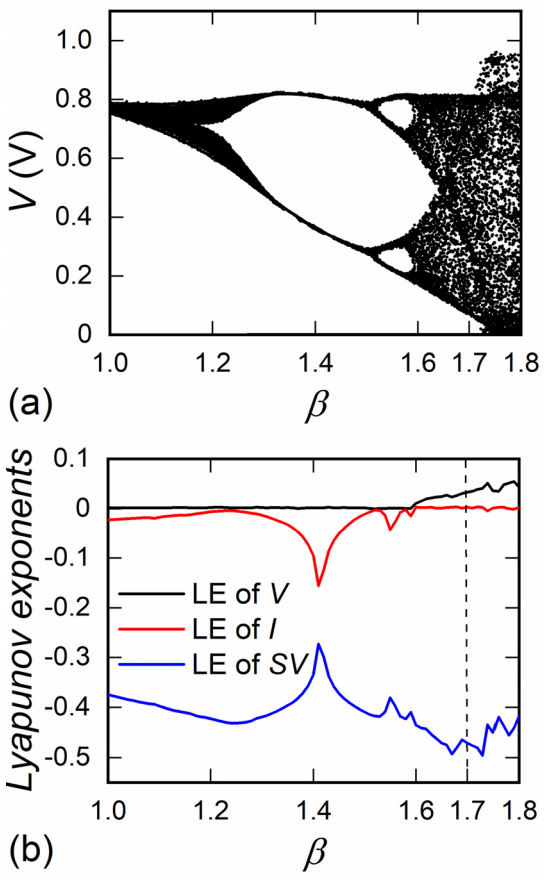

FIGURE 5. Solved evolutions of (a) bifurcation diagram of V and (b) three Lyapunov exponents (LEs) with β by using MO-MIHAM.

The comparisons in Figs. 6(a)–6(d) show MO-MIHAM4 solutions of ODEs (38) are also in line with RKF45 solutions, further verifying the high accuracy and wide applicability of MO-MIHAM. Moreover, for small variations of initial conditions [δ, SV (0), V_1 (0), and V_2 (0)], MO-MIHAM4 accurately tracks the different dynamic behaviors, i.e., single attractor [Fig. 6(a)], coexisting chaotic attractors [Fig. 6(b)], coexisting bifurcation modes [Fig. 6(c)], and period doubling bifurcation [Fig. 6(d)]. These observations further show our method is cable of tracking the influences of small variations of initial conditions, in a more complicated memristive circuit than MCL.

Additionally, it is clear from $dSV(t)/dt = -\delta SV - \rho V_1$ in (38) that the memristor in BPF circuit is a voltage-controlled memristor according to Chua's definition [48], instead of the current-controlled memristor in MCL circuit, this difference also validates the wide applicability of MO-MIHAM from the views of physical mechanism and model of memristor.

V. DISCUSSION

A. ACCURACY

It is known from (15)–(18) that the convergence control parameters vector $\hbar_i$ in each subinterval are optimized, due to the applications of minimum *discrete squared residual errors* of ODEs and MO (e.g. TOPSIS in this paper). The faster $\hbar_i$ approach to its optimal value, the faster non-inferior analytic approximate solution $u_{i,r,N}(t)$ converges to its exact solution, and hence guaranteeing the accuracy of $u_{i,r,N}(t)$ in the relating subinterval. Namely, the non-inferior optimizations in subinterval are performed by using $\hbar_i$ and TOPSIS for getting the corresponding non-inferior accuracy. Then, because the complete analytical solution $u_{S,r,N}(t)$ of $u_r(t)$ for the time span I is essentially composed of solutions in subintervals [see (19) and (20)], its corresponding *discrete squared residual error* and, thus, accuracy, are also non-inferior in I.

In spite of these non-inferior characteristics, MO-MIHAM using TOPSIS still has higher accuracy compared with traditional homotopy-based analytical methods without using MO, as shown in Tables 2–4. Theoretically, if the number of subinterval S tends to infinity [see (19) and (20)], the analytical approximate solution solved by using MO-MIHAM will infinitely close to the exact solution (if it exists), even under low approximation order N.

B. TRADEOFF BETWEEN ACCURACY AND COMPUTATIONAL COMPLEXITY

MO-MIHAM, likes other traditional approximation theories [29], [31], [32], [36], [37], also needs to make a reasonable tradeoff between accuracy and computational complexity.

Note that, complexity here is evaluated by the execution time and memory cost for simulation. To be specific, the number of subintervals S (negatively correlated with the time step size $\Delta t = I/S$) and the approximation order N should be increased to achieve higher approximation accuracy. Increasing these two parameters, unfortunately, would also increase the complexity of final solution expression [see (36)], which is inconvenient for analytical analysis. However, because of its high accuracy as shown in Figs. 3–5 and Tables 2–4, MO-MIHAM allows the choices of small S and N and large time step Δt for a chaotic system (in this paper, $S = 1000$, $N = 4$, and $\Delta t = I/S = 0.1$), showing the reasonable tradeoff. Namely, under a given accuracy requirement, MO-MIHAM enables higher efficiency and hence lower computational complexity, compared with other analytical methods in this paper. Table 5 shows the comparisons of computational complexities among different methods, verifying the above analyses. It is clear from Table 5 that, the execution time of MO-MIHAM is the highest compared with other methods, due to the introductions of $\hbar_i$ in each subinterval and corresponding MO. However, the accuracy of MO-MIHAM (i.e., *RMSE*) is also the highest. Namely, MO-MIHAM has high accuracy at the expense of execution time and, thus, complexity.

To evaluate computational performance more objectively, we introduced the Quality Factor equal to *RMSE*×execution time. From Table 5, we see the Quality Factor of MO-MIHAM4 is the lowest, indicting MO-MIHAM is superior to other methods for the comprehensive

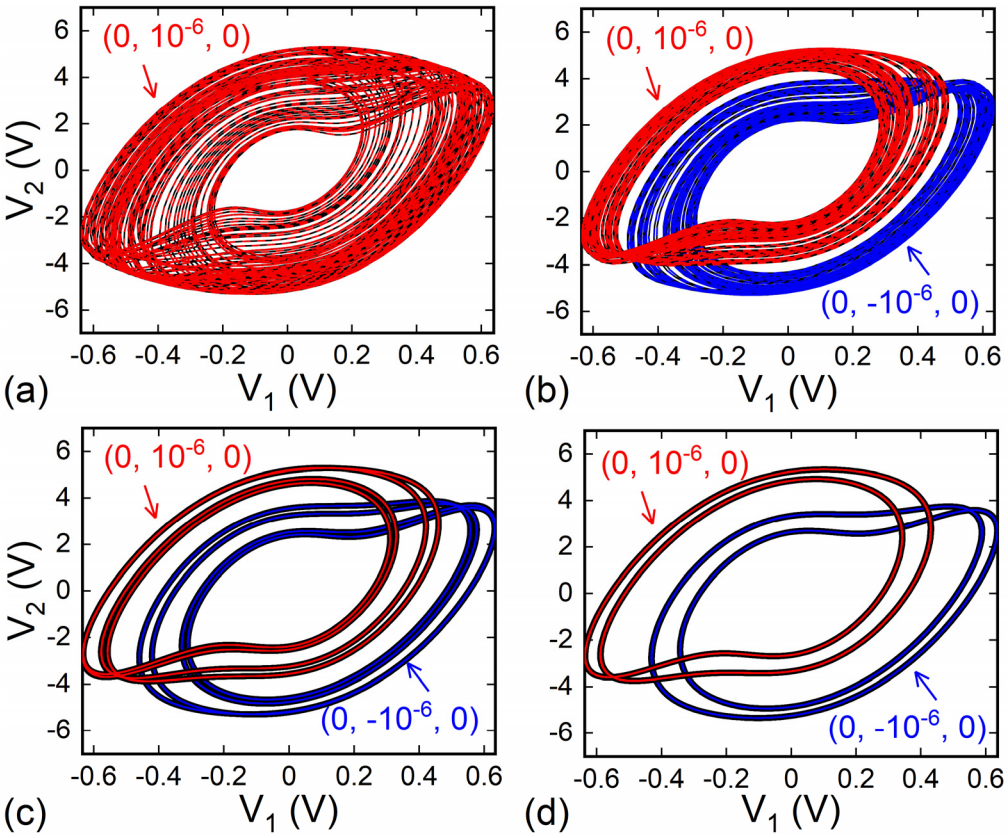

FIGURE 6. Comparisons of phase portraits solved by MO-MIHAM4 and by RKF45 with different dynamics control parameter δ, in the V_1–V_2 plane. Black solid lines are RKF45 solutions, while colored (red and blue) dash lines are MO-MIHAM4 solutions. (a) Chaotic attractor for $\delta = 8$. (b) Coexisting chaotic attractors for $\delta = 8.6$. (c) Coexisting period-4 limit cycles for $\delta = 9$. (d) Coexisting period-2 limit cycles for $\delta = 9.5$. $(0, 10^{-6}, 0)$ and $(0, -10^{-6}, 0)$ are initial conditions of (SV, V_1, V_2). All the related simulation parameters are the same as those in Fig. 2 except the initial conditions.

TABLE 5. Comparisons of computational complexities of different methods for solving *SV* in MCL circuit.

Error parameters	HPM4 [25]	HAM4 [35]	MuHPM4 [29]	MO-MIHAM4
RMSE	29989.3	1.08532	0.0569286	**0.0226105**
Execution time (s)	0.12	19.85	134.22	**220.91**
Memory cost (MB)	46.8797	65.6751	85.3281	**94.3284**
Quality Factor*	3598.716	21.54360	7.640957	**4.994886**

*Quality Factor = *RMSE*× execution time.

consideration of accuracy and computational complexity, under the same approximation order $N = 4$. For other approximation orders, we have the same results, which are not listed here due to the limited space.

C. SCALABILITY

MO-MIHAM has high scalability due to the following reasons:

1) OTHER MO METHODS

TOPSIS is used to simultaneously minimize *discrete squared residual errors* of ODEs for optimizing $\hbar_i$ in this paper [see (15)–(18)]. Although TOPSIS [38] has several drawbacks [39], e.g., the problem of ranking reversal, and although the solution derived from TOPSIS is non-inferior, we still obtain more accurate solutions by using TOPSIS-based MO-MIHAM, compared with solutions solved by other homotopy-based methods without using TOPSIS. This is an interesting attempt, showing the superiority of MO-MIHAM.

To further explore the potential performance and application of MO-MIHAM, within its framework, researchers could replace TOPSIS with other more efficient MO methods, such as currently developed TOPSIS [55]–[58], extended TOPSIS integrating with other MO techniques [59], [60], and intelligent optimization algorithms (including Multiple Objective Genetic algorithm [61]–[64], Multiple Objective Swam Intelligence algorithm [65]–[67], Multiple Objective immune algorithm [64], etc.).

2) OTHER APPLICATIONS AND ACCELERATION METHODS OF SOLVING $\hbar_i$

In this paper, we focus the applications of MO-MIHAM not only on the classical MCL circuit but also on the current memristive BPF chaotic circuit (these circuits have different

memristor models and circuit classifications), so the proposed MO-MIHAM, theoretically, has potential for extending to other chaotic systems. This is because MO-MIHAM is based on the commonly used HAM that is an effective and general mathematical method for solving various ODE [42], [45]–[48] and on the extensive MO methods described in Section V. C. 1).

It also should be noted that convergence control parameter $\hbar_i$ is derived from the *discrete squared residual error* in this paper, other convergence accelerating methods having less computational complexity and execution time are also compatible with MO-MIHAM, such as Ratio method [68] and Weierstrass-M discriminant method [69]. By using these methods, $\hbar_i$ can be obtained more efficiently and hence the Quality Factor of MO-MIHAM can be further reduced.

VI. CONCLUSION

In summary, we have proposed a novel analytical method called MO-MIHAM for tracking the chaotic trajectories of memristive circuits. By comparing solutions derived from MO-MIHAM with traditional homotopy-based analytical methods (i.e., HPM, HAM, and MuHPM), we found the major advantage of MO-MIHAM is the higher approximation accuracy and, thus, higher computational performance (i.e., lower Quality Factor). Additionally, MO-MIHAM enables both qualitative and quantitative analyses and high freedom to choose homotopy-related terms, and it is insensitive to convergence issues. Moreover, the solutions derived from MO-MIHAM can be easily integrated into Electronic Design Automation (EDA) software for circuit synthesis. With theoretical analyses and circuital applications of MO-MIHAM, we have verified that the combination of multi-interval HAM and Multi-objective Optimization is feasible. Theoretically, MO-MIHAM may has potential for applications in other chaotic systems, due to its high scalability.

APPENDIX

This section shows the detailed solution procedures of MCL system (22) for the first two subintervals ($i = 1$ and 2) of $x_{i,N}(t)$, $y_{i,N}(t)$, and $z_{i,N}(t)$. Note that all the significant digit of solved solution is kept to 6.

(1) $i = 1$.

Firstly, we chose $t_0 = 0$, $x_{1,0}(t) = V(0) = 0.1$, $y_{1,0}(t) = I(0) = 0.1$, $z_{1,0}(t) = SV(0) = 0$, $S = 1000$ (i.e., the time step of subinterval $\Delta t = I/S = 0.1$), and $N = 4$ (the reasons for choices of S, Δt, and N were explained in detail in Section V. B). These values and other parameters values are all given in Table 1. Secondly, according to the flow of Algorithm 1 and the detailed solution procedure mentioned above, and taking into consideration of the unknown $\hbar_1 = \{\hbar_{1,1}, \hbar_{1,2}, \hbar_{1,3}\}$, we obtained the incomplete fourth-order analytical approximate solutions of three variables: $x_{1,4}(t, \hbar_1)$, $y_{1,4}(t, \hbar_1)$, and $z_{1,4}(t, \hbar_1)$, in the first subinterval I_1. Thirdly, based on (16)–(18), we solved the associated convergence-control parameters in $\hbar_1$ as $\hbar_{1,1} = -0.991140$, $\hbar_{1,2} = -0.920402$, and $\hbar_{1,3} = -1.09231$, respectively. And finally, substituting the solved $\hbar_1$ into $x_{1,4}(t, \hbar_1)$, $y_{1,4}(t, \hbar_1)$, and $z_{1,4}(t, \hbar_1)$, we derived the complete fourth-order closed solutions of three variables in the original MCL circuit equations (22) as follows [in which $x = V(t)$, $y = I(t)$, and $z = SV(t)$]:

$$\begin{cases} x_{1,4}(t) = 0.100000 + 0.099999t + 0.010600t^2 \\ \qquad\quad - 0.0032247t^3 - 0.00017494t^4 \\ y_{1,4}(t) = 0.100000 + 0.0212113t - 0.00968963t^2 \\ \qquad\quad - 0.00286490t^3 + 0.000447384t^4 \\ z_{1,4}(t) = -0.0999927t - 0.00559066t^2 \\ \qquad\quad + 0.00271071t^3 - 0.00794557t^4. \end{cases} \tag{A1}$$

It should be emphasized that the above expressions are in line with the solution definitions employing polynomial base functions (24), proving above solution procedure is valid.

(2) $i = 2$.

From the definition of subinterval, (5), and Table 1, time step in second subinterval I_2 is Δt =0.1, initial time in I_2 is $t_{2,0} = t_0 + \Delta t \times (2-1) = 0.1$, the initial value of solutions in the subinterval I_2 are $x_{2,0} = x_{1,4}(t_{2,0}) = 0.110103$, $y_{2,0} = y_{1,4}(t_{2,0}) = 0.102021$, and $z_{2,0} = z_{1,4}(t_{2,0}) = -0.0100533$, which are derived from (A1). And then, using a procedure similar to I_1, we obtained $\hbar_{2,1} = -1.01971$, $\hbar_{2,2} = -0.893526$, $\hbar_{2,3} = -1.00172$ and

$$\begin{cases} x_{2,4}(t) = 0.0999999 + 0.100001 + 0.0106025872t^2 \\ \qquad\quad - 0.00326892t^3 - 0.000551529t^4 \\ y_{2,4}(t) = 0.100000 + 0.0212122t - 0.00970592t^2 \\ \qquad\quad - 0.00288226t^3 + 0.000106714t^4 \\ z_{2,4}(t) = -0.100002t - 0.00560192t^2 \\ \qquad\quad + 0.00274990t^3 + 0.000188834t^4. \end{cases} \tag{A2}$$

We can see the above expressions also match (24) well.

(3) For $2 < i \leq S = 1000$.

The procedures, similar to those of I_1 and I_2, are repeated until $i = S = 1000$.

REFERENCES

[1] W. Marszalek and J. Sadecki, "Complex two-parameter bifurcation diagrams of a simple oscillating circuit," *IEEE Trans. Circuits Syst., II, Exp. Briefs*, vol. 66, no. 4, pp. 687–691, Apr. 2019.

[2] J. Ma, F. Wu, A. Alsaedi, and J. Tang, "Crack synchronization of chaotic circuits under field coupling," *Nonlinear Dyn.*, vol. 93, no. 4, pp. 2057–2069, Sep. 2018.

[3] A. Buscarino, C. Corradino, L. Fortuna, and L. O. Chua, "Taming spatiotemporal chaos in forced memristive arrays," *IEEE Trans. Very Large Scale Integr. (VLSI) Syst.*, vol. 26, no. 12, pp. 2947–2954, Dec. 2018.

[4] D. B. Strukov, G. S. Snider, D. R. Stewart, and R. S. Williams, "The missing memristor found," *Nature*, vol. 453, pp. 80–83, May 2008.

[5] M. A. Zidan, J. P. Strachan, and W. D. Lu, "The future of electronics based on memristive systems," *Nature Electron.*, vol. 1, no. 1, pp. 22–29, Jan. 2018.

[6] B. Bao, N. Wang, Q. Xu, H. Wu, and Y. Hu, "A simple third-order memristive band pass filter chaotic circuit," *IEEE Trans. Circuits Syst., II, Exp. Briefs*, vol. 64, no. 8, pp. 977–981, Aug. 2017.

[7] H. Bao, N. Wang, B. Bao, M. Chen, P. Jin, and G. Wang, "Initial condition-dependent dynamics and transient period in memristor-based hypogenetic jerk system with four line equilibria," *Commun. Nonlinear Sci. Numer. Simul.*, vol. 57, pp. 264–275, Apr. 2018.

[8] X. Zhong, M. Peng, M. Shahidehpour, and S. Guo, "Bifurcation and periodic solutions in memristive hyperchaotic system," *IEEE Access*, vol. 6, pp. 23202–23212, Apr. 2018.
[9] S. F. Wang, "Dynamical analysis of memristive unified chaotic system and its application in secure communication," *IEEE Access*, vol. 6, pp. 66055–66061, Oct. 2018.
[10] Z. Guo, J. Wang, and Z. Yan, "Global exponential synchronization of two memristor-based recurrent neural networks with time delays via static or dynamic coupling," *IEEE Trans. Syst., Man, Cybern., Syst.*, vol. 45, no. 2, pp. 235–249, Feb. 2015.
[11] Y. Xin, Y. Li, X. Huang, and Z. Cheng, "Quasi-synchronization of delayed chaotic memristive neural networks," *IEEE Trans. Cybern.*, vol. 49, no. 2, pp. 712–718, Feb. 2019.
[12] J. Liu and R. Xu, "Adaptive synchronisation of memristor-based neural networks with leakage delays and applications in chaotic masking secure communication," *Int. J. Syst. Sci.*, vol. 49, no. 6, pp. 1300–1315, 2018.
[13] L. Wang, T. Dong, and M.-F. Ge, "Finite-time synchronization of memristor chaotic systems and its application in image encryption," *Appl. Math. Comput.*, vol. 347, pp. 293–305, Apr. 2019.
[14] G. Peng and F. Min, "Multistability analysis, circuit implementations and application in image encryption of a novel memristive chaotic circuit," *Nonlinear Dyn.*, vol. 90, no. 3, pp. 1607–1625, Nov. 2017.
[15] Z. Wang and X. Wang, "A novel memristor-based circuit implementation of full-function Pavlov associative memory accorded with biological feature," *IEEE Trans. Circuits Syst. I, Reg. Papers*, vol. 65, no. 7, pp. 2210–2220, Jul. 2018.
[16] J. Grollier, D. Querlioz, and M. D. Stiles, "Spintronic nanodevices for bioinspired computing," *Proc. IEEE*, vol. 104, no. 10, pp. 2024–2039, Oct. 2016.
[17] V. T. Pham, S. Jafari, S. Vaidyanathan, C. Volos, and X. Wang, "A novel memristive neural network with hidden attractors and its circuitry implementation," *Sci. China Technol. Sci.*, vol. 59, no. 3, pp. 358–363, Mar. 2015.
[18] Q, Xu, Q. L. Zhang, B. C. Bao, and Y. H. Hu, "Non-autonomous second-order memristive chaotic circuit," *IEEE Access*, vol. 5, pp. 21039–21045, Jul. 2017.
[19] Q. Hong, Q. Wu, X. Wang, and Z. Zeng, "Novel nonlinear function shift method for generating multiscroll attractors using memristor-based control circuit," *IEEE Trans. Very Large Scale Integr. (VLSI) Syst.*, vol. 27, no. 5, pp. 1174–1185, May 2019.
[20] G. Zhang and Y. Shen, "Exponential stabilization of memristor-based chaotic neural networks with time-varying delays via intermittent control," *IEEE Trans. Neural Netw. Learn. Syst.*, vol. 26, no. 7, pp. 1431–1441, Jul. 2015.
[21] V. Ntinas, A. Ascoli, R. Tetzlaff, and G. C. Sirakoulis, "A complete analytical solution for the on and off dynamic equations of a TaO memristor," *IEEE Trans. Circuits Syst. II, Exp. Briefs*, vol. 66, no. 4, pp. 682–686, Apr. 2019.
[22] F. Corinto and M. Forti, "Memristor circuits: Flux—Charge analysis method," *IEEE Trans. Circuits Syst. I, Reg. Papers*, vol. 63, no. 11, pp. 1997–2009, Nov. 2016.
[23] T. Wang and J. Roychowdhury, "Well-posed models of memristive devices," May 2016, *arXiv:1605.04897*. [Online]. Available: https://arxiv.org/abs/1605.04897
[24] D. Biolek, Z. Biolek, V. Biolkova, and Z. Kolka, "Modeling of TiO_2 memristor: From analytic to numerical analyses," *Semicond. Sci. Technol.*, vol. 29, no. 12, Nov. 2014, Art. no. 125008.
[25] C. Hernández-Mejía, A. Sarmiento-Reyes, and H. Vázquez-Leal, "A novel modeling methodology for memristive systems using homotopy perturbation methods," *Circuits Syst. Signal Process.*, vol. 36, no. 3, pp. 947–968, Mar. 2017.
[26] P. J. Hilton, *An Introduction to Homotopy Theory*. Cambridge, U.K.: Cambridge Univ. Press, 1953.
[27] A. Sarmiento-Reyes, L. Hernández-Martínez, H. Vázquez-Leal, C. Hernández-Mejía, and G. U. D. Arango, "A fully symbolic homotopy-based memristor model for applications to circuit simulation," *Anal. Integr. Circuits Signal Process.*, vol. 85, no. 1, pp. 65–80, Oct. 2015.
[28] H. Vazquez-Leal, "Path tracking of dynamics of a chaotic memristor circuit," *J. Interpolation Approx. Sci. Comput.*, vol. 2014, pp. 1–18, May 2014.
[29] M. S. H. Chowdhury, I. Hashim, and S. Momani, "The multistage homotopy-perturbation method: A powerful scheme for handling the Lorenz system," *Chaos, Solitons Fractals*, vol. 40, no. 4, pp. 1929–1937, May 2009.
[30] J.-H. He, "A coupling method of a homotopy technique and a perturbation technique for non-linear problems," *Int. J. Non-Linear Mech.*, vol. 35, no. 1, pp. 37–43, Jan. 2000.
[31] J.-H. He, "Homotopy perturbation method: A new nonlinear analytical technique," *Appl. Math. Comput.*, vol. 135, no. 1, pp. 73–79, Feb. 2003.
[32] J.-H. He, "An elementary introduction to the homotopy perturbation method," *Comput. Math. Appl.*, vol. 57, no. 3, pp. 410–412, Feb. 2009.
[33] M. Turkyilmazoglu, "Some issues on HPM and HAM methods: A convergence scheme," *Math. Comput. Model.*, vol. 53, nos. 9–10, pp. 1929–1936, May 2011.
[34] M. Turkyilmazoglu, "Is homotopy perturbation method the traditional Taylor series expansion," *Hacettepe J. Math. Statist.*, vol. 44, no. 3, pp. 651–657, May 2015.
[35] S. J. Liao, "Systematic descriptions and related theorems," in *Homotopy Analysis Method in Nonlinear Differential Equations*, vol. 6. Berlin, Germany: Springer, 2012, ch. 4, sec. 1, pp. 135–187.
[36] S. J. Liao, "Notes on the homotopy analysis method: Some definitions and theorems," *Commun. Nonlinear Sci. Numer. Simul.*, vol. 14, no. 4, pp. 983–997, Apr. 2009.
[37] S. J. Liao, "An optimal homotopy-analysis approach for strongly nonlinear differential equations," *Commun. Nonlinear Sci. Numer.*, vol. 15, no. 8, pp. 2003–2016, Aug. 2010.
[38] C.-L. Hwang and K. Yoon, "Methods for multiple attribute decision making," in *Multiple Attribute Decision Making* (Lecture Notes in Economics and Mathematical Systems). Berlin, Germany: Springer, 1981.
[39] E. K. Zavadskas, A. Mardani, Z. Turskis, A. Jusoh, and K. M. D. Nor, "Development of TOPSIS method to solve complicated decision-making problems—An overview on developments from 2000 to 2015," *Int. J. Inf. Technol. Decis. Making*, vol. 15, no. 3, pp. 645–682, May 2016.
[40] *Mathematica 11.2*. Accesed: Jun. 5, 2018. [Online]. Available: https://www.wolfram.com/
[41] S. J. Liao, "The proposed homotopy analysis technique for the solution of nonlinear problems," Ph.D. dissertation, School Nav. Archit. Ocean Eng., Shanghai Jiaotong Univ., Shanghai, China, 1992.
[42] S. J. Liao, "Chance and challenge: A brief review of homotopy analysis method," in *Advances in the Homotopy Analysis Method*, vol. 3. Singapore: World Scientific, 2013, ch. 1, sec. 2, pp. 103–160.
[43] S. Liao, "On the homotopy analysis method for nonlinear problems," *Appl. Math. Comput.*, vol. 147, no. 2, pp. 499–513, Jan. 2004.
[44] C. Nash, S. Sen, and J. Stachel, "Topology and geometry for physicists," *Amer. J. Phys.*, vol. 54, no. 5, p. 476, May 1986. doi: 10.1119/1.14570.
[45] S. Kumar and M. M. Rashidi, "New analytical method for gas dynamics equation arising in shock fronts," *Comput. Phys. Commun.*, vol. 185, no. 7, pp. 1947–1954, Jul. 2014.
[46] Y. Zhao, Z. Lin, and S. Liao, "An iterative HAM approach for nonlinear boundary value problems in a semi-infinite domain," *Comput. Phys. Commun.*, vol. 184, no. 9, pp. 2136–2144, Sep. 2013.
[47] A. C. Cullen and S. R. Clarke, "A fast, spectrally accurate homotopy based numerical method for solving nonlinear differential equations," *J. Comput. Phys.*, vol. 385, pp. 106–118, May 2019.
[48] S. Vong and Z. Wang, "A compact difference scheme for a two dimensional fractional Klein–Gordon equation with Neumann boundary conditions," *J. Comput. Phys.*, vol. 274, pp. 268–282, Oct. 2014.
[49] J. Branke, K. Deb, H. Dierolf, and M. Osswald, "Finding knees in multi-objective optimization," in *Parallel Problem Solving from Nature*. Berlin, Germany: Springer, 2004.
[50] D. H. Wolper and W. G. Macready, "No free lunch theorems for optimization," *IEEE Trans. Evol. Comput.*, vol. 1, no. 1, pp. 67–82, Apr. 1997.
[51] B. Muthuswamy and L. O. Chua, "Simplest chaotic circuit," *Int. J. Bifurcation Chaos*, vol. 20, no. 5, pp. 1567–1580, 2010.
[52] L. O. Chua, "The fourth element," *Proc. IEEE*, vol. 100, no. 6, pp. 1920–1927, Jun. 2012.
[53] E. Fehlberg, "Klassische runge-kutta-formeln vierter und niedrigerer ordnung mit schrittweiten-kontrolle und ihre anwendung auf Wärmeleitungsprobleme," *Computing*, vol. 6, nos. 1–2, pp. 61–71, Mar. 1970.
[54] W. H. Enright, K. R. Jackson, S. P. Nørsett, and P. G. Thomsen, "Interpolants for Runge-Kutta formulas," *ACM Trans. Math. Softw.*, vol. 12, no. 3, pp. 193–218, Sep. 1987.
[55] K. Kumar and H. Garg, "TOPSIS method based on the connection number of set pair analysis under interval-valued intuitionistic fuzzy set environment," *Comput. Appl. Math.*, vol. 37, no. 2, pp. 1319–1329, May 2016.

[56] F. Shen, X. Ma, Z. Li, Z. Xu, and D. Cai, "An extended intuitionistic fuzzy TOPSIS method based on a new distance measure with an application to credit risk evaluation," *Inf. Sci.*, vol. 428, pp. 105–119, Feb. 2018.
[57] M. S. A. Khan, S. Abdullah, M. Y. Ali, I. Hussain, and M. Farooq, "Extension of TOPSIS method base on Choquet integral under interval-valued Pythagorean fuzzy environment," *J. Intell. Fuzzy Syst.*, vol. 34, no. 1, pp. 267–282, Jan. 2018.
[58] W. Chen, Y. Shen, and Y. Wang, "Evaluation of economic transformation and upgrading of resource-based cities in Shaanxi province based on an improved TOPSIS method," *Sustain. Cities Soc.*, vol. 37, pp. 232–240, Feb. 2018.
[59] G. Tian, H. Zhang, M. Zhou, and Z. Li, "AHP, gray correlation, and TOPSIS combined approach to green performance evaluation of design alternatives," *IEEE Trans. Syst., Man, Cybern., Syst.*, vol. 48, no. 7, pp. 1093–1105, Jul. 2018.
[60] B. C. Ervural, S. Zaim, O. F. Demirel, Z. Aydin, and D. Delen, "An ANP and fuzzy TOPSIS-based SWOT analysis for Turkey's energy planning," *Renew. Sustain. Energy Rev.*, vol. 82, pp. 1538–1550, Feb. 2018.
[61] E. Zitzler and L. Thiele, "Multiobjective evolutionary algorithms: A comparative case study and the strength Pareto approach," *IEEE Trans. Evol. Comput.*, vol. 3, no. 4, pp. 257–271, Nov. 1999.
[62] A. Konak, D. W. Coit, and A. E. Smith, "Multi-objective optimization using genetic algorithms: A tutorial," *Rel. Eng. Syst. Saf.*, vol. 91, no. 9, pp. 992–1007, Sep. 2006.
[63] K. Deb, A. Pratap, S. Agarwal, and T. Meyarivan, "A fast and elitist multiobjective genetic algorithm: NSGA-II," *IEEE Trans. Evol. Comput.*, vol. 6, no. 2, pp. 182–197, Apr. 2002.
[64] X. Wang, L. Gao, C. Zhang, and X. Shao, "A multi-objective genetic algorithm based on immune and entropy principle for flexible job-shop scheduling problem," *Int. J. Adv. Manuf. Technol.*, vol. 51, nos. 5–8, pp. 757–767, Nov. 2010.
[65] B. Xue, M. Zhang, and W. N. Browne, "Particle swarm optimization for feature selection in classification: A multi-objective approach," *IEEE Trans. Cybern.*, vol. 43, no. 6, pp. 1656–1671, Dec. 2013.
[66] B. Yagmahan and M. M. Yenisey, "Ant colony optimization for multi-objective flow shop scheduling problem," *Comput. Ind. Eng.*, Apr. 2008, vol. 54, no. 3, pp. 411–420.
[67] I. C. Trelea, "The particle swarm optimization algorithm: Convergence analysis and parameter selection," *Inf. Process. Lett.*, vol. 85, no. 6, pp. 317–325, Mar. 2003.
[68] M. Turkyilmazoglu, "An effective approach for evaluation of the optimal convergence control parameter in the homotopy analysis method," *Filomat*, vol. 30, no. 6, pp. 1633–1650, Jan. 2016.
[69] M. Turkyilmazoglu, "Convergence accelerating in the homotopy analysis method: A new approach," *Adv. Appl. Math. Mech.*, vol. 10, no. 4, pp. 925–947, Jun. 2018.

WEI HU received the B.S. and M.S. degrees in microelectronics from Xidian University, Xi'an, China, in 2006 and 2009, respectively. He is currently pursuing the Ph.D. degree with Fuzhou University, Fuzhou, China, where he has been a Research Assistant with the College of Physics and Information Engineering, since 2010. His research interests include modeling and application of innovative memristive devices systems, design of high performance analog, and mixed-signal integrated circuit.

HAIBO LUO received the B.E. degree in communication engineering from the Wuhan University of Technology, China, in 2006, the M.E. degree in information and communication engineering from Hunan University, China, in 2009, and the Ph.D. degree from Fuzhou University, Fuzhou, China, in 2018.

He is currently an Assistant Professor with Minjiang University. His research interests include the Internet of Things.

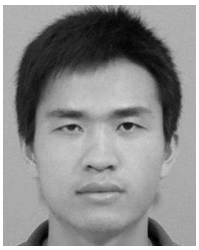

CHUANDONG CHEN received the M.A. degree in microelectronics from Fuzhou University, Fuzhou, China, in 2008.

He is currently a Lecturer with Fuzhou University. His research interest includes design for test of digital IC.

RONGSHAN WEI received the B.S. and Ph.D. degrees in microelectronics from Tsinghua University, Beijing, China, in 2003 and 2008, respectively.

He is currently a Professor with Fuzhou University. His research interest includes analog circuits design.